Experiments and numerical results on non-linear vibrations of an impacting Hertzian contact. Part 2: random excitation

J. Perret-Liaudet, E. Rigaud*

Laboratoire de Tribologie et Dynamique des Systèmes UMR 5513, 36 Ave. Guy de Collongue, F-69134 Ecully Cedex, France

Received 13 February 2002; accepted 1 July 2002

Abstract

Non-linear dynamic behaviour of a normally excited preloaded Hertzian contact (including possible contact losses) is investigated using an experimental test rig. It consists of a double sphere plane contact loaded by the weight of a rigid moving mass. Contact vibrations are generated by a external Gaussian white noise and exhibit vibroimpact responses when the input level is sufficiently high. Spectral contents and statistics of the stationary transmitted normal force are analyzed. A single-degree-of-freedom non-linear oscillator including loss of contact and Hertzian non-linearities is built for modelling the experimental system. Theoretical responses are obtained by using the stationary Fokker–Planck equation and also Monte Carlo simulations. When contact loss occurrence is very occasional, numerical results show a very good agreement with experimental ones. When vibroimpacts occur, results remain in reasonable agreement with experimental ones which justify the modelling and the numerical methods described in this paper.

The contact loss non-linearity appears to be rather strong compared to the Hertzian non-linearity. It actually induces a large broadening of the spectral contents of the response. This result is of great importance in noise generation for many systems such as mechanisms using contacts to transform motions and forces (gears, ball-bearings, cam systems, to name a few). It is also of great importance for tribologists preoccupied with preventing surface damage.
© 2002 Elsevier Ltd. All rights reserved.

1. Introduction

Hertzian contacts exist in many mechanical systems such as mechanisms and machines (gears, cam systems, rolling element bearings, etc). Under operating conditions, these contacts are often excited by dynamic normal forces superimposed on a mean static load. These excitation forces

which are deterministic or random, can result from external sources, such as applied load fluctuations, or from internal ones, such as roughness-induced vibrations. Under excessive excitation, contacts can exhibit undesirable vibroimpact responses, allowed by clearances introduced through manufacturing tolerances. Resulting dynamic behaviour is characterized by intermittent loss of contact and shocks leading to excessive wear, surface damage and excessive noise.

In a companion paper (Part I: harmonic excitation) [1], the dynamic behaviour of a fundamental preloaded Hertzian contact subjected to harmonic normal forces was studied. To this end, an improved experimental test rig permitted us to investigate the primary resonance in detail, including vibroimpact responses. Theoretical results were also presented to analyse the main characteristics of the primary resonance.

In the present second part of this work, the previous analysis is extended to the case of vibroimpact response of a preloaded and non-sliding dry Hertzian contact under Gaussian white random normal excitation. Comparisons between experimental and theoretical results leads to some conclusions regarding some characteristics of the random dynamic responses, including vibroimpact behaviour.

As the literature shows, there exist a few papers in this area. These include Refs. [2–8]. They generally concern random normal vibrations for sliding contacts related to the internal random roughness surface induced excitation.

Experimental results can be found for example in Refs. [3–6,8]. In these studies, random force excitation applied to the contact is never exactly known because measurements are always performed during sliding conditions. It is estimated on the basis of assumptions on the spatial spectrum of the surface roughness input. Decrease of the frequency domain spectrum shape with a ω^{-4} law is generally retained. These works principally focus on the interaction between normal and tangential forces, friction force vibrations and friction coefficient behaviour under dynamic conditions. Further, vibroimpact behaviours are very partially analyzed.

In a theoretical point of view, Nayak [2] presents a detailed analysis of a Hertzian contact excited by a broadband random normal force. But, intermittent loss of contact is partially taken into account. This problem is examined by Hess et al. [6] who consider also small values of probability of contact loss. The theoretical method used is based on the Fokker–Planck equation, introducing the restoring elastic Hertzian force by a third order Taylor expansion. The procedure is refined by Pärssinen in a recent brief paper by introducing the real form of the theoretical restoring elastic Hertzian force [7].

2. Test rig and experimental procedure

The experimental system studied is similar to the one presented in Part I of this work [1]. Recall that it consists of a 25.4 mm diameter steel ball preloaded between two horizontal steel flat surfaces. The first one is rigidly fixed to a vertically moving cylinder, the second one is rigidly fixed to a heavy rigid frame. The double sphere–plane dry contact is loaded by a static normal load F_s = mg = 110 N which corresponds to the weight of the moving cylinder.

Using a suspended vibration exciter, random normal force is applied to the moving cylinder and superimposed on the static load. For this end, a signal generator and a power amplifier are used to

generate the white-noise signal. This signal is filtered above 1 kHz which is up to four times the experimental linearized contact frequency ($f_0 = 233.4$ Hz).

A piezoelectric force transducer is mounted between the vibration exciter and the moving cylinder to measure the excitation force. The normal force $N(t)$ transmitted to the base through the contact is measured by a piezoelectric force transducer mounted between the lower plane and the rigid frame. Considering the experimental system and the transducer stiffness (8000 N/μm), the force measurement bandwidth is sufficiently wide (0–7 kHz).

The input force and the dynamic response are displayed on a storage oscilloscope. Experimental average one-sided RMS magnitude spectra are measured with a real-time spectrum analyzer using a sampling rate of 4096 samples over the frequency bandwidth (0–1 kHz) with a frequency resolution always less than 0.25 Hz. Average spectra were obtained with a number of spectrum up to 275. Dynamic responses are digitized using an A/D converter and stored for statistical post-treatments. These responses are sampled for a 20 s duration with sampling rate of 10 000 samples per second.

3. The theoretical dynamic model

3.1. Equation of motion

On the basis of identical assumptions that were introduced in the first part of this work, the experimental system is modelled by a randomly excited single-degree-of-freedom non-linear dynamic system shown in Fig. 1 and is described by the following motion equation [9]:

$$m\ddot{z} + c\dot{z} + k[z\mathrm{H}(z)]^{3/2} = F_s(1 + \sqrt{h}W(t)).$$ (1)

In this equation, z is the normal displacement of the rigid mass m measured such that $z < 0$ corresponds to loss of contact. Assuming a viscous law, c is a damping coefficient, k is a constant given by the Hertzian theory, H is the Heaviside step function, $W(t)$ is a stationary zero-mean Gaussian white noise and h controls level of the random normal force. From Eq. (1), the theoretical static contact compression z_s and the linearized contact natural circular frequency Ω are given by

$$z_s = \left(\frac{F_s}{k}\right)^{2/3},$$ (2)

$$\Omega^2 = \left(\frac{3k}{2m}\right)z_s^{1/2}.$$ (3)

Recall that data have been previously found from the experimental characteristics as

$$z_s = 7\,\mu\text{m}, \quad f_0 = \frac{\Omega}{2\pi} = 232\,\text{Hz}$$ (4, 5)

Now, by letting

$$q = \frac{3}{2}\left(\frac{z - z_s}{z_s}\right), \quad \tau = \Omega t, \quad \varpi = \omega/\Omega$$ (6, 7, 8)
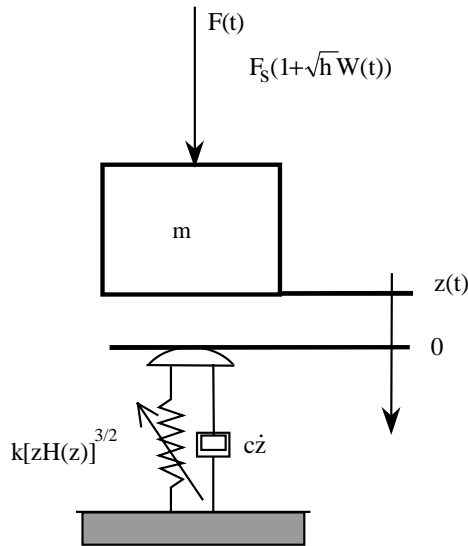
Fig. 1. The studied randomly excited single-degree-of-freedom oscillator.

a dimensionless equation of motion is achieved in the same way as in Part I:

$$\ddot{q} + 2\zeta\dot{q} + [(1 + \tfrac{2}{3}q)\mathrm{H}(1 + \tfrac{2}{3}q)]^{3/2} = 1 + \sqrt{h}w(\tau). \tag{9}$$

In this equation, overdot indicates differentiation with respect to the dimensionless time τ, ζ is an equivalent viscous damping ratio, parameter h controls the input level and $w(\tau)$ is chosen as a stationary zero-mean Gaussian white noise with a unit power spectral density, $S_{ww}(\varpi) = 1$.. So, considering the dimensionless excitation force $f(\tau) = \sqrt{h}w(\tau)$, the power spectral density and autocorrelation function are given by

$$S_{ff}(\varpi) = h, \tag{10}$$

$$R_{ff}(\tau) = 2\pi h\delta(\tau), \tag{11}$$

where $\delta(\tau)$ is the Dirac function. With this choice, one should notice that the power spectral density of $W(t)$ is equal to $1/\Omega$. Hence, the power spectral density of the excitation $F(t) = F_s\sqrt{h}W(t)$ is equal to

$$S_{ff}(\omega) = S_0 = F_s^2 h/\Omega. \tag{12}$$

From the experimental one-sided spectral density $G_{ff}(f) = G_0$, one has

$$G_0 = 4\pi S_0, \quad h = \frac{f_0 G_0}{2F_s^2}. \tag{13, 14}$$

Finally, it should be noted from Eq. (9) that loss of contact corresponds to the inequality

$$q < -\tfrac{3}{2}. \tag{15}$$

3.2. Numerical methods

To investigate theoretical dynamic responses, several numerical methods have been used as follows:

- a classical numerical time integration explicit scheme, i.e., the central difference scheme, for achieving dynamic time histories of responses,
- the stationary Fokker–Planck equation applied to system (6) under Gaussian white-noise excitation for describing the statistics of the dynamic responses,
- classical statistical tools to describe random vibrations,
- Monte Carlo simulations to estimate power spectral densities of responses of the randomly excited system.

When necessary, these methods are described in the following.

4. Experimental results

4.1. Dynamics without loss of contact

Fig. 2 displays the experimental average one-sided RMS magnitude spectra of the transmitted normal force for various random input levels. These levels are chosen in such a way that no loss of contact occurs during the measure. For these cases, $G_0 = 1 \times 10^{-4}$, $G_0 = 4.5 \times 10^{-3}$ and $G_0 = 30 \times 10^{-3}$ N^2/Hz with corresponding values $h = 1 \times 10^{-6}$, 4.5×10^{-5} and 3×10^{-4}, For the lowest input level, the spectrum exhibits a single resonant peak close to the linearized contact frequency
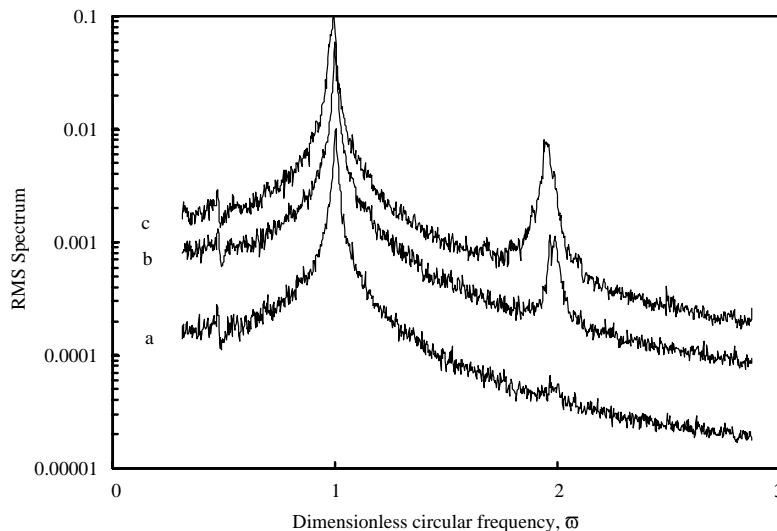
Fig. 2. Experimental one-sided RMS spectra of the transmitted normal force for $h \approx 1 \times 10^{-6}$, 4.5×10^{-5} and 3×10^{-4} (respectively a, b, c).

(233.4 Hz). This result is in very good agreement with the predicted one (232 Hz). In this case, linear behaviour can be assumed and an equivalent viscous damping ratio can be estimated from the half-power frequency bandwidth method. Experimental curve leads to ζ less than 0.5%. This result is coherent with the previous value found in the Part I of this work [1].

When the input level increases, the dynamic behaviour becomes weakly non-linear. Actually, a second peak close to the second harmonic of the linearized contact frequency arises. For the highest input level shown in Fig. 2, the second peak value reaches 8% of the main peak value. Furthermore, increasing the input level, one observes a weak broadening of the two peaks. A weak decrease of the two peak frequencies is also observed.

Experimental normal force probability density functions corresponding to the three preceding input levels are presented in Fig. 3. The associated mean, standard deviation, and skewness values are given in Table 1. The normal force shows a nearly zero probability of intermittent contact loss (which corresponds to $N < -1$). Further, increasing the input level, the Gaussian-like shape of the probability density function moves to a more and more asymmetrical shape. This is confirmed by the evolution of the skewness value given in Table 1. However, the deviation from a Gaussian process is weak. Considering the mean value of the normal force, it remains also very close to the applied static load. Further, the standard deviation reaches 40% of the static normal force.

Fig. 4 displays an example of the time history of the normal force for an input level such that intermittent contact loss does not occur during acquisition data. In agreement with the spectral
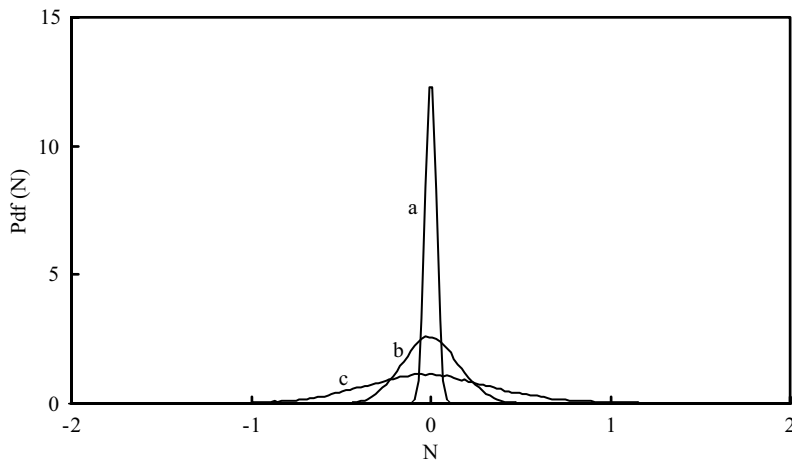

Fig. 3. Probability density functions of the measured transmitted normal force for $h \approx 1 \times 10^{-6}$, 4.5×10^{-5} and 3×10^{-4} (respectively a, b, c).

Table 1
Mean value $E[N]$, standard deviation σ, and skewness γ of the measured dimensionless transmitted force

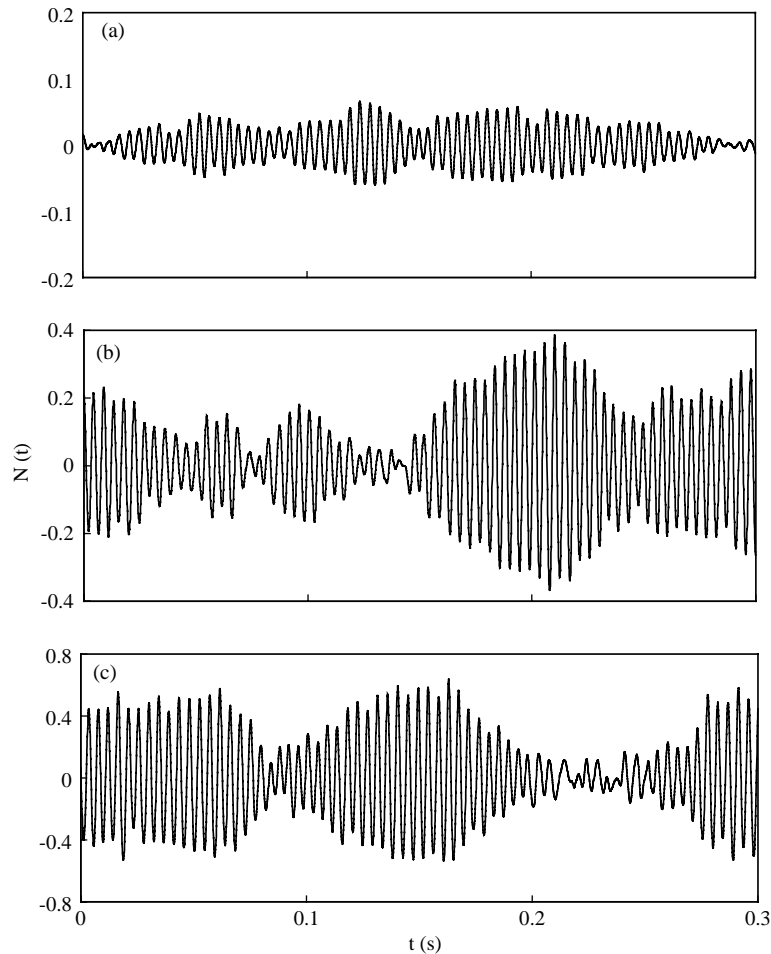| h	$E[N]$	σ	γ
1.0×10^{-6}	-9.8×10^{-5}	0.03	0.011
4.5×10^{-5}	7.0×10^{-6}	0.15	0.089
3.0×10^{-4}	4.6×10^{-5}	0.38	0.260

Fig. 4. Time traces of the transmitted normal force $h \approx 1 \times 10^{-6}$, 4.5×10^{-5} and 3×10^{-4} (respectively a, b, c).

responses content, this trace is typical of a narrow-frequency-band random noise response. A slightly asymmetrical response can be observed, revealing the asymmetric law of the restoring Hertzian elastic force around the static load.

4.2. Dynamics with intermittent loss of contact

When the random input level increases, intermittent contact loss may occur as the normal force can reach the static load. Fig. 5 shows the experimental average one-sided RMS magnitude spectra for increasing random input levels, chosen in such a way that intermittent loss of contact occurs during the measure. For these cases, $G_0 = 6 \times 10^{-2}$, $G_0 = 1.7 \times 10^{-1}$ and $G_0 = 2.5 \times 10^{-1}$ N^2/Hz with corresponding values $h = 6 \times 10^{-4}$, 1.7×10^{-3} and 2.5×10^{-3}. The broadening of the resonant peaks is clearly observed. It is known that it is an essential property of spectrum shapes with large non-linearity and low damping [10]. One can also observe the rising of a broad third peak.
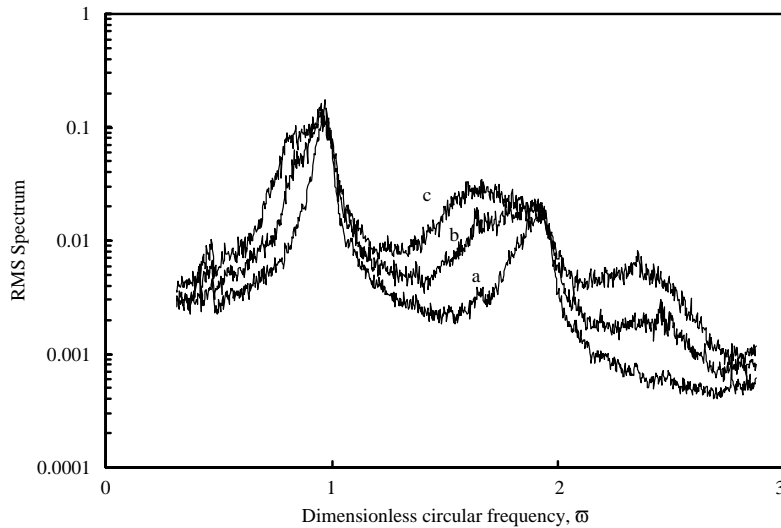
Fig. 5. Experimental one-sided RMS spectra of the transmitted normal force for $h \approx 6 \times 10^{-4}$, 1.7×10^{-3} and 2.5×10^{-3} (respectively a, b, c).
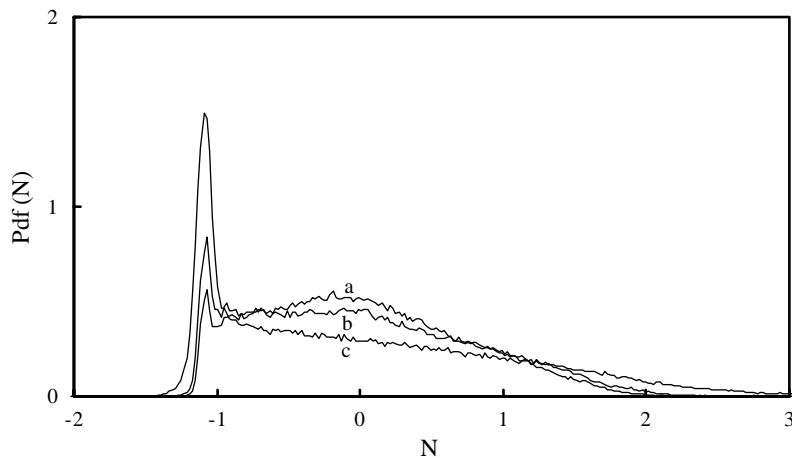

Fig. 6. Probability density functions of the measured transmitted normal force for $h \approx 6 \times 10^{-4}$, 1.7×10^{-3} and 2.5×10^{-3} (respectively a, b, c).

Furthermore, resonant peaks shift to lower frequencies, particularly the second and the third ones. This can be explained by the more and more asymmetrical shape of the time trace of the transmitted force induced by the flight response of the cylinder. Hence, as expected, loss of contact non-linearity is stronger than the Hertzian contact one.

Fig. 6 displays the corresponding experimental normal force probability density functions. The associated mean value, standard deviation and skewness values are given in Table 2. Probability density functions are strongly asymmetrical and hardly deviate from a Gaussian process. This is

Table 2
Mean value $E[N]$, standard deviation σ and skewness γ of the measured dimensionless transmitted force

h	$E[N]$	σ	γ
6.0×10^{-4}	-2.1×10^{-4}	0.70	0.406
1.7×10^{-3}	-3.4×10^{-4}	0.78	0.464
2.5×10^{-3}	-2.4×10^{-4}	1.01	0.758

Table 3
Loss of contact duration

h	Total loss of contact duration (%)	Number of loss of contact during 20 s	Mean period of cylinder fly (ms)
6.0×10^{-4}	3	693	0.9
1.7×10^{-3}	6	1050	1.1
2.5×10^{-3}	15	2227	1.5

confirmed by skewness values given in Table 2. Asymmetric behaviour corresponds to the appearance of a peak at the zero transmitted normal force in the probability density functions ($N = -1$). In particular, the longer flight time of the cylinder, the higher the peak is. Calculation of the peak area allows estimation of the total loss of contact duration (this has been also estimated by treating time histories with coherent results). Results are reported in Table 3. For the highest input level, intermittent contact loss occurs during approximately 15% of the overall time.

Fig. 7 displays an example of the time history of the normal force for an input level such that intermittent contact loss occurs. From time traces, the total number of contact losses during the acquisition time (20 s) is measured. The mean period of the cylinder flight is also estimated. The results are presented in Table 3. For the highest input level, this mean period is approximately equal to 1.5 ms and the number of impacts becomes large (around 2200 during an observation time of 20 s).

5. Theoretical results

5.1. The stationary Fokker–Planck equation

Assuming stationary Gaussian white-noise excitation, statistics of the stationary response can be obtained using the Fokker–Planck equation [2,6,7,11]. To this end, consider the following second order non-linear differential equation of motion, in the general form

$$\ddot{q} + 2\zeta\dot{q} + G(q) = f(\tau), \tag{16}$$

where $f(\tau)$ is a zero mean stationary Gaussian white-noise excitation with intercorrelation function $R_{ff}(\tau) = 2\pi h\delta(\tau)$, i.e., a power spectral density $S_{ff}(\varpi) = h$. $G(q)$ represents the non-linear restoring
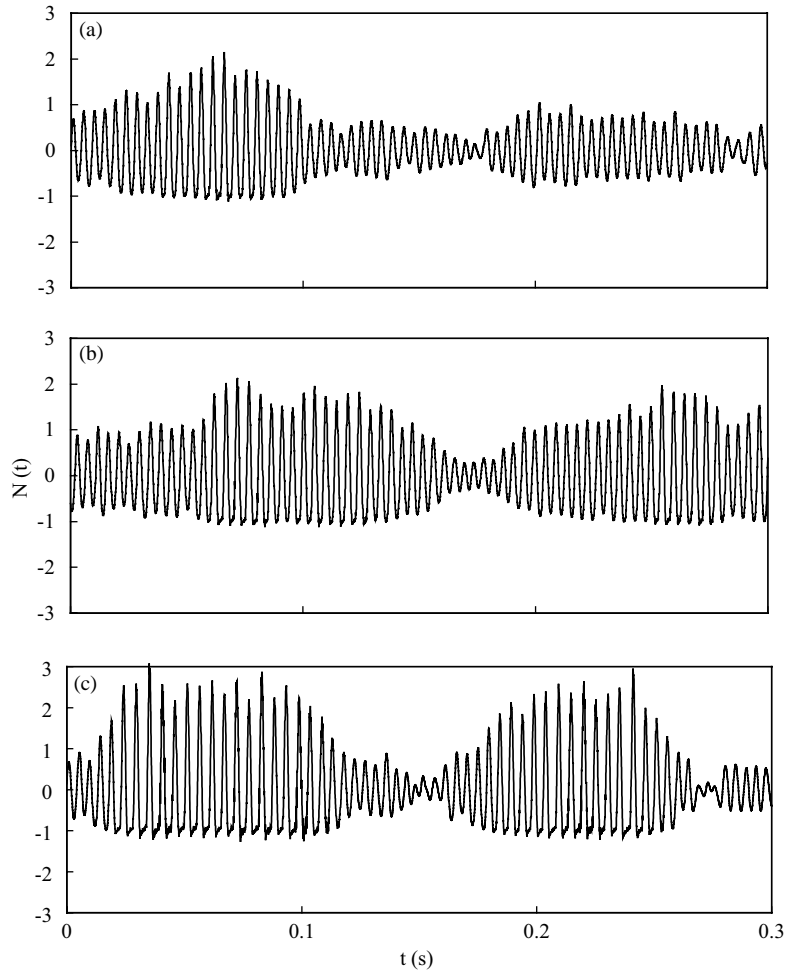
Fig. 7. Time traces of the transmitted normal force for $h \approx 6 \times 10^{-4}$, 1.7×10^{-3} and 2.5×10^{-3} (respectively a, b, c).

force including the non-linearity related to contact loss. The forward Fokker–Planck equation which governs the transitional probability density function $p(q, \dot{q}, t | q_0, \dot{q}_0)$ of system (16) is obtained as follows:

$$\frac{\partial p}{\partial t} + \dot{q}\frac{\partial p}{\partial q} = \frac{\partial}{\partial \dot{q}}[2\zeta\dot{q}p + G(q)p] + \pi h\frac{\partial^2 p}{\partial \dot{q}^2}. \tag{17}$$

Considering the stationary case and after some rearrangements, the stationary joint probability density function $p_s(q, \dot{q})$ satisfies

$$\frac{\partial}{\partial \dot{q}}\left[G(q)p_s + \frac{\pi h}{2\zeta}\frac{\partial p_s}{\partial q}\right] + \left(2\zeta\frac{\partial}{\partial \dot{q}} - \frac{\partial}{\partial q}\right)\left[\dot{q}p_s + \frac{\pi h}{2\zeta}\frac{\partial p_s}{\partial \dot{q}}\right] = 0. \tag{18}$$

Hence, a solution is achieved by requiring

$$\left[G(q)p + \frac{\pi h}{2\zeta}\frac{\partial p}{\partial q}\right] = 0 \tag{19}$$

and

$$\left[\dot{q}p + \frac{\pi h}{2\zeta}\frac{\partial p}{\partial \dot{q}}\right] = 0. \tag{20}$$

From Eqs. (19) and (20), one easily obtains a solution for the stationary joint probability density function $p_s(q, \dot{q})$ as

$$p_s(q,\dot{q}) = A\exp\left\{\frac{-2\zeta}{\pi h}\frac{\dot{q}^2}{2}\right\}\exp\left\{\frac{-2\zeta}{\pi h}\int_0^q G(s)\,\mathrm{d}s\right\}, \tag{21}$$

where A is a constant which normalizes the density function. From Eq. (21), marginal densities for the displacement and the velocity appear statistically independent and a closed form for the displacement probability density function $p_q(q)$ is easily achieved as follows:

$$p_q(q) = C\exp\left\{\frac{-2\zeta}{\pi h}\int_0^q G(s)\,\mathrm{d}s\right\} \tag{22}$$

or from expression of $G(q)$:

$$\begin{cases} p_q(q) = C\exp\left\{-\frac{2\zeta}{\pi h}\left[\frac{3}{5}\left(1+\frac{2}{3}q\right)^{5/2}-q-\frac{3}{5}\right]\right\} & \text{if } q > -\frac{3}{2}, \\ p_q(q) = C\exp\left\{-\frac{2\zeta}{\pi h}\left[-q-\frac{3}{5}\right]\right\} & \text{if } q \leqslant -\frac{3}{2}, \end{cases} \tag{23}$$

where C is a constant which normalizes the marginal density function.

As one can see in Eq. (21), marginal density function for the velocity is a Gaussian process:

$$p_{\dot{q}}(\dot{q}) = B\exp\left\{\frac{-2\zeta}{\pi h}\frac{\dot{q}^2}{2}\right\}, \tag{24}$$

where B is a constant which normalizes the marginal density function.

By using numerical integration methods, statistical moments of the displacement $q(\tau)$ are computed from the probability density function (23):

$$E[q^n(\tau)] = \int_{-\infty}^{+\infty} q^n p_q(q)\,\mathrm{d}q. \tag{25}$$

Since the relation between the displacement $q(\tau)$ and the elastic restoring force $N(\tau)$ is known, the probability density function of the elastic restoring force $p_N(N)$ is derived in a classical manner [12].

Consider the relation $N = G(q)$:

$$\begin{cases} N = \left(1+\frac{2}{3}q\right)^{3/2}-1 & \text{if } q > -\frac{3}{2}, \\ N = -1 & \text{if } q \leqslant -\frac{3}{2}. \end{cases} \tag{26}$$

If q_i, $i = 1,...,r$, are all real roots of Eq. (26), one obtains the probability density function of the elastic restoring force as

$$p_N(N) = \sum_{i=1}^{r} \frac{p_q(q_i)}{|N'(q_i)|},$$ (27)

where $N'(q)$ is the derivative of N with respect to q.

Finally

$$\begin{cases} p_N(N) = (1+N)^{-1/3} p_q\left(\frac{3}{2}(1+N)^{2/3} - \frac{3}{2}\right) & \text{if } N > -1, \\ p_N(-1) = \delta(-1) \int_\infty^{-3/2} p_q(s)\,\mathrm{d}s, & \\ p_N(N) = 0 & \text{if } N < -1, \end{cases}$$ (28)

where δ is the Dirac delta function. Notice that p_N is zero for $N < -1$, and contains an impulse at $N = -1$ of area equal to the probability of loss of contact. Notice also that

$$\lim_{\substack{N \to -1 \\ N > -1}} p_N(N) = +\infty.$$ (29)

Statistical moments are given as follows:

$$E[N^n(\tau)] = \int_{-\infty}^{+\infty} N^n p_N(N)\,\mathrm{d}N$$ (30)

from which mean value, standard deviation and skewness values can be derived.

5.2. Monte Carlo simulations

Monte Carlo simulations have been performed to estimate the response spectral densities of the randomly excited system. For this end, an explicit numerical time integration scheme (central difference method) has been used for solving the motion equation (9) and for achieving dynamic time histories of the normal force. Spectra were obtained via a Fast Fourier Transform procedure with number of samples equal to 2048. Average spectra were obtained with a number of spectrum up to 400. To simulate the Gaussian white-noise external force, a sufficiently wide band limited pseudo-random signal has been considered

$$w(\tau) = W_M \sum_{k=1}^{k=M} \cos(\varpi_k \tau + \phi_k)$$ (31)

Frequencies ϖ_k are independent and uniformly distributed in $[0, \varpi_{\max}]$ and W_M is a coefficient which takes into account the frequency resolution

$$W_M = \sqrt{\Delta f . h}$$ (32)

Choosing phases

$$\phi_k = 2\pi \sqrt{-2r_1} \cos(2\pi r_2),$$ (33)

where r_1 and r_2 are two random numbers uniformly distributed over $[0,1]$, the signal is normally distributed.

Also, Monte Carlo simulations have been used to obtain statistics of the stationary responses treating the theoretical time histories. Statistical moments have been estimated over 10^5 times the period of the linearized system with up to 250 samples by period.

5.3. Theoretical results

5.3.1. Statistics of the stationary response

The probability densities of the elastic restoring force are shown in Fig. 8 ($h = 3 \times 10^{-6}$, 8×10^{-5}, 5×10^{-4}) and Fig. 9 ($h = 1.2 \times 10^{-3}$, 2×10^{-3}, 3.2×10^{-3}) for increasing input levels and for a damping ratio equal to 0.5%. The two figures correspond, respectively, to input levels chosen in such a way that no loss of contact occur. By comparing Fig. 8 with Fig. 3, both results derived from the Fokker–Planck equation and the Monte Carlo simulations are in good agreement with
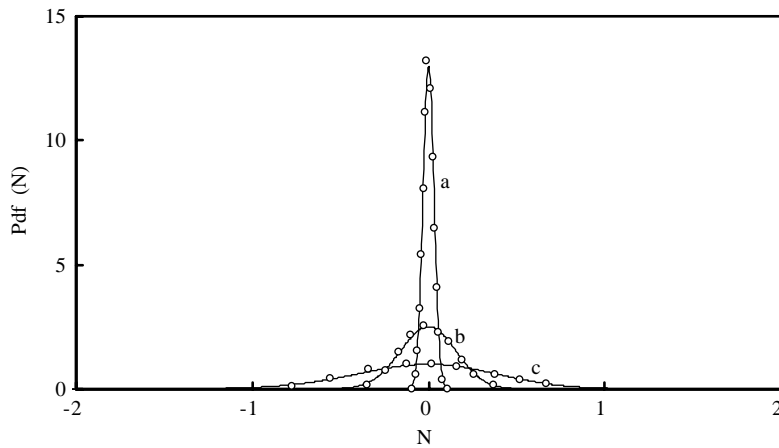

Fig. 8. Probability density functions of the elastic restoring force for $h \approx 3 \times 10^{-6}$, 8×10^{-5} and 5×10^{-4} (respectively a, b, c). Results obtained from the stationary Fokker–Planck equation (—) and from Monte Carlo simulations (○).

Fig. 9. Probability density functions of the elastic restoring force for $h \approx 1.2 \times 10^{-3}$, 2×10^{-3} and 3.2×10^{-3} (respectively a, b, c). Results obtained from the stationary Fokker–Planck equation (—) and from Monte Carlo simulations (○).

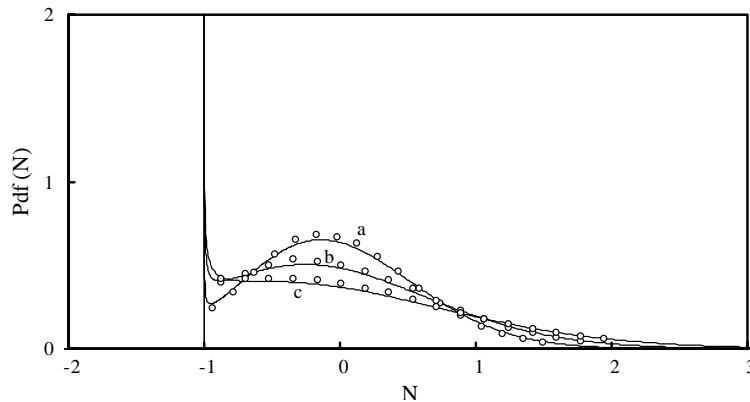experimental results. Small differences observed in Fig. 9 can result from numerical errors associated to the estimation of the Dirac value at $N = -1$. Actually, the introduced input levels leading to the same probability density function shapes are not exactly the same but appear to be of the same order. Moreover, it should be stated that the pertinent variable is the ratio between damping ratio and input level (see Eq. (21)). Further, the damping law as well as damping value are not exactly known particularly when the amplitude response grows. So, in the authors' opinion, adjusting damping ratio gives no more satisfaction than adjusting input level. However, one can assume that the experimental damping ratio of 0.5% is overestimated. Actually, by taking into account the average ratio between the two series of input levels, one can conclude that a damping ratio equal to 0.3% is more convenient. By comparing Fig. 9 with Fig. 6, one can conclude that a satisfactory agreement between experimental and numerical results also exists when intermittent contact losses occur. Of course, the theoretical infinite value and Dirac function at $N = -1$ cannot be observed in the experimental case. Further, ball motion between the two planes associated to the second mode and clearly experimentally observed (see Fig. 7) is a source of discrepancy between theoretical and experimental probability density functions. Numerical statistics obtained from Eq. (25) are given in Table 4. Statistical results obtained from Monte Carlo simulations are reported in Table 5. Concerning standard deviations, in accordance with the preceding remarks, the authors have found that the satisfactory agreement between measured and computed results (see Tables 1 and 2) becomes very good if the input level is scaled by the damping ratio with a value equal to 0.3%. So, one can conclude that the numerical tools used in this study are suitable for describing standard deviations, even if the probability density function

Table 4
Mean value $E[N]$, standard deviation σ and skewness γ of the computed dimensionless transmitted force by using the Fokker–Planck equation

h	$E[N]$	σ	γ	$p\ (q < -1.5)$ (%)
3×10^{-6}	-1.57×10^{-3}	0.03	-0.010	≈ 0
8×10^{-5}	-4.23×10^{-3}	0.16	-0.054	≈ 0
5×10^{-4}	-2.81×10^{-2}	0.40	-0.157	≈ 0
1.2×10^{-3}	-1.33×10^{-3}	0.60	0.502	2
2.0×10^{-3}	-1.66×10^{-3}	0.75	0.710	7
3.2×10^{-3}	-2.14×10^{-3}	0.91	0.951	15

Table 5
Mean value $E[N]$, standard deviation σ and skewness γ of the computed dimensionless transmitted force by using Monte Carlo simulations

h	$E[N]$	σ	γ
3×10^{-6}	-3.0×10^{-4}	0.03	0.018
8×10^{-5}	-1.0×10^{-3}	0.15	0.097
5×10^{-4}	-2.0×10^{-3}	0.38	0.260
1.2×10^{-3}	-4.1×10^{-3}	0.57	0.490
2.0×10^{-3}	-4.2×10^{-3}	0.72	0.666
3.2×10^{-3}	-4.4×10^{-3}	0.88	0.917

is not exactly the same when contact losses occur. Concerning mean values, discrepancy between experimental results and numerical ones is found. However, it should be pointed out that the numerical mean values remain very close to the static applied load which is coherent with experimental data. Further, samplings of both experimental time traces and those obtained from Monte Carlo simulations are perhaps not sufficient to ensure precise estimate of the mean value. Concerning skewness values, good agreement between experimental and Monte Carlo simulations results is obtained, but discrepancies appear with results obtained from the Fokker–Planck equation. The authors do not have a precise explanation, but can assume that the sampling procedure leads to numerical errors for estimating skewness values. Finally, probabilities of contact loss given in Table 4 have been computed from Eq. (23). Again, very good agreement with experimental results is observed (compare the total loss of contact duration given in Table 3).

5.3.2. Response spectra

Fig. 10 and 11 display the numerical average one-sided RMS magnitude spectra for increasing input levels ($h = 3 \times 10^{-6}$, 8×10^{-5}, 5×10^{-4}, 1.2×10^{-3}, 2×10^{-3}, 3.2×10^{-3}). Comparisons with Fig. 2 and 5 reveal a very good agreement between experimental and numerical results when intermittent contact losses do not occur. The agreement remains satisfactorily when contact losses occur, even if experimental level of the second and third peaks are higher than those obtained from numerical simulations.

Since the experimental test rig does not permit higher input levels, it can be interesting to know the effect of increasing input level on the transmitted force response through numerical simulations. Fig. 12 displays the average one-sided RMS magnitude spectra of the elastic restoring force for input levels higher than the preceding ones. The result is a large broadening of the spectral density response, in such a way that preceding peaks completely disappear.
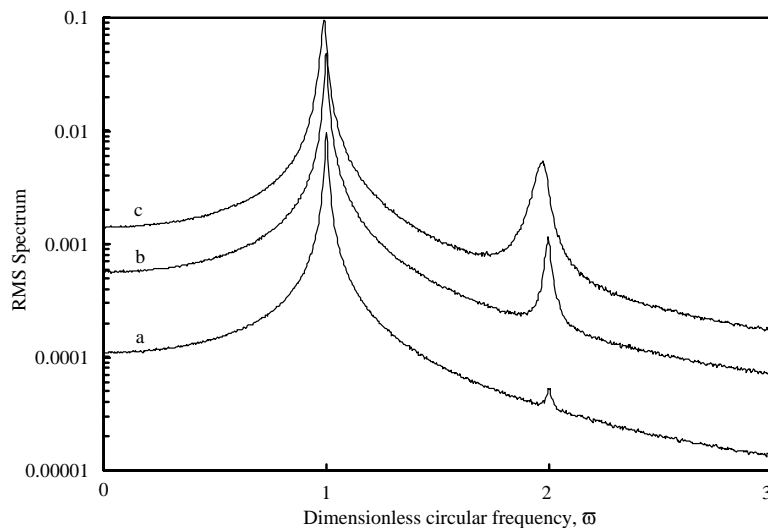

Fig. 10. Numerical one-sided RMS spectra of the elastic restoring force for $h \approx 3 \times 10^{-6}$, 8×10^{-5} and 5×10^{-4} (respectively a, b, c).
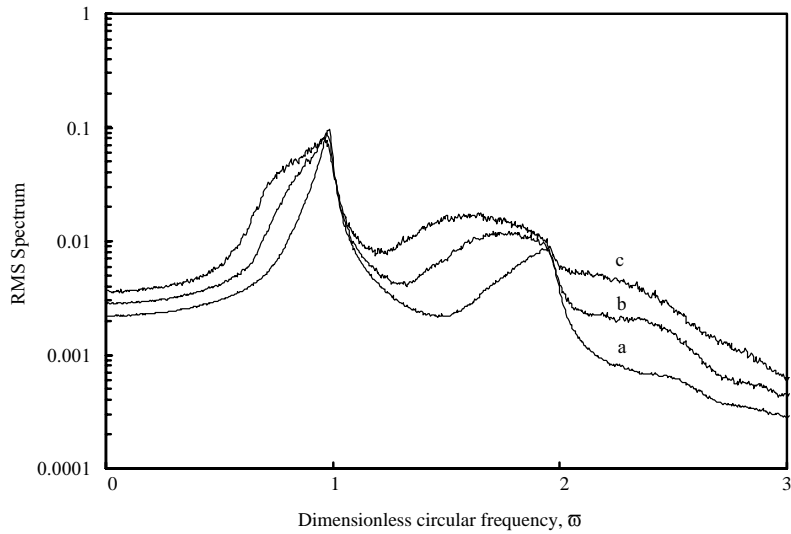
Fig. 11. Numerical one-sided RMS spectra of the elastic restoring force for $h \approx 1.2 \times 10^{-3}$, 2×10^{-3} and 3.2×10^{-3} (respectively a, b, c).
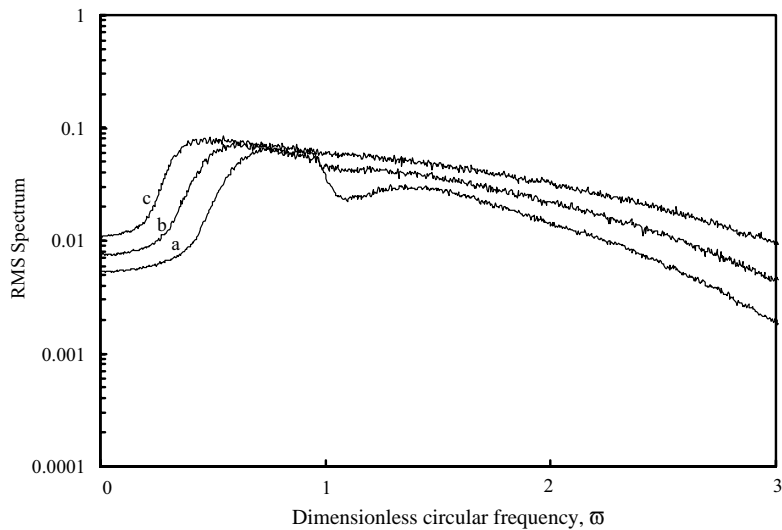

Fig. 12. Numerical one-sided RMS spectra of the elastic restoring force for $h \approx 7 \times 10^{-3}$, 1.4×10^{-2} and 3×10^{-1} (respectively a, b, c).

5.3.3. Effect of the Hertzian contact law on response spectra

Since a linear restoring force law is introduced in many modelling of practical systems, it is of interest to compare results between models which include the Hertzian contact law and those which do not. For this end, consider a simplified model for describing the elastic restoring force as
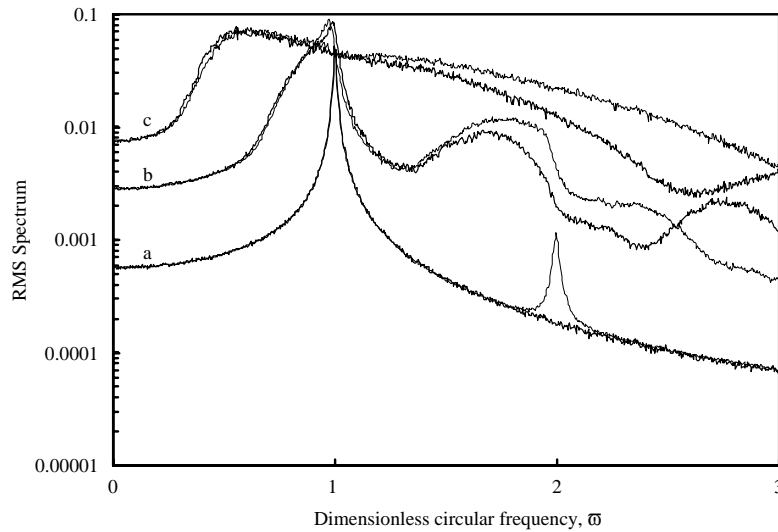
Fig. 13. Numerical one-sided RMS spectra of the elastic restoring force obtained with an Hertzian elastic contact law (thin line) and a linear one (thick line) for $h \approx 8 \times 10^{-5}$, 2×10^{-3} and 1.4×10^{-2} (respectively a, b, c).

follows:

$$N = (1 + q)H(1 + q) - 1. \tag{34}$$

Fig. 13 displays the numerical average one-sided RMS magnitude spectra for three input levels ($h = 8 \times 10^{-5}$, 2×10^{-3}, 1.4×10^{-2}) showing comparisons between results obtained from the two models. Identical results are obtained around the primary peak. In contrast, the simplified model is not suitable to describe the dynamic behaviour in the range of higher frequencies. Depending on the objective, approximation (34) can be favourably introduced under the cover of saving of time consumed.

6. Conclusions

An experimental test rig consisting of a dry double sphere–plane Hertzian contact is modelled as a non-linear single-degree-of-freedom system. Non-linear normal force response of this randomly excited system is analyzed through experimental and theoretical results.

For very low input force amplitude, almost linear behaviour is observed, and the experimental linearized contact frequency is deduced with a very good agreement with the predicted one. Equivalent viscous damping ratio is less than 0.5%. Increasing the input amplitude reveals the second harmonic spectral peak. Probability density functions of the response show a little deviation from a Gaussian process resulting from the Hertzian non-linearity as long as intermittent contact loss is very occasional.

As the input level increases, the probability of intermittent loss of contact strongly increases. The probability density functions of the response become largely asymmetrical. Furthermore, the rising of the third harmonic spectral peak and the broadening of spectral peaks are

observed. This last behaviour is known as an essential property of the power spectral density of systems with large non-linearity and low damping. It is clearly verified in the experimental results.

For all these behaviours, numerical and experimental results agree. It is concluded that the associated theoretical model is sufficiently accurate, despite the fact that damping is modelled in a very simple way. So, compared to vibrations under harmonic excitation, precise knowledge of the damping law during vibroimpact response is less determining. Also, the stationary Fokker–Planck equation and Monte Carlo simulations are suitable methods for describing the dynamic behaviour of the impacting Hertzian contact under normal random excitation.

In future, further numerical and experimental works are planned to take into account the effect of a lubricating film and the effect of sliding surfaces.

Acknowledgements

Appendix A. Nomenclature

m	rigid moving mass
c	damping coefficient
k	constant obtained from Hertzian theory
F_s	static load
$F(t)$	excitation normal force
$W(t)$	Gaussian white-noise process
h	parameter controlling input level
$z(t)$	normal displacement
Z_s	static contact compression
Ω	linearized natural circular frequency
f_0	linearized natural frequency
ζ	damping ratio
τ	dimensionless time
$q(\tau)$	dimensionless normal displacement
$f(\tau)$	dimensionless excitation normal force
$w(\tau)$	dimensionless Gaussian white-noise process
ω	circular frequency
ϖ	dimensionless circular frequency
$N(\tau)$	Hertzian elastic restoring force
$S_{xx}(\omega)$	power spectral density of x
$G_{xx}(\omega)$	one-sided power spectral density of x
$R_{xx}(\tau)$	intercorrelation function of x
$p_x(x)$	probability density function of x

$E[x]$, $\bar{x}$ mean value of x
σ standard deviation
γ skewness value

References

[1] E. Rigaud, J. Perret-Liaudet, Experiments and numerical results on nonlinear vibrations of an impacting Hertzian contact. Part 1: harmonic excitation, Journal of Sound and Vibration 265 (2) (2003) 289–307, this issue.

[2] R. Nayak, Contact vibrations, Journal of Sound and Vibration 22 (3) (1972) 297–322.

[3] A. Soom, C. Kim, Interactions between dynamic normal and frictional forces during unlubricated sliding, American Society of Mechanical Engineers Journal of Lubrication Technology 105 (1983) 221–229.

[4] A. Soom, C. Kim, Roughness-induced dynamic loading at dry and boundary lubricated sliding contacts, American Society of Mechanical Engineers Journal of Lubrication Technology 105 (1983) 514–517.

[5] A. Soom, J.-W. Chen, Simulation of random surface roughness-induced contact vibrations at Hertzian contacts during steady sliding, American Society of Mechanical Engineers Journal of Tribology 108 (1986) 123–127.

[6] D. Hess, A. Soom, C. Kim, Normal vibrations and friction at a Hertzian contact under random excitation: theory and experiments, Journal of Sound and Vibration 153 (3) (1992) 491–508.

[7] M. Pärssinen, Hertzian contact vibrations under random external excitation and surface roughness, Journal of Sound and Vibration 214 (4) (1998) 779–783.

[8] J. Sabot, P. Krempf, C. Janolin, Non linear vibrations of a sphere–plane contact excited by a normal load, Journal of Sound and Vibration 214 (2) (1998) 359–375.

[9] K. Johnson, Contact Mechanics, Cambridge University Press, Cambridge, 1979.

[10] R. Bouc, The power spectral density of response for a strongly non-linear random oscillator, Journal of Sound and Vibration 175 (3) (1994) 317–331.

[11] T. Caughey, Derivation and application of the Fokker–Planck equation to discrete nonlinear dynamic systems subjected to white random excitation, Journal of Acoustical Society of America 35 (1963) 1683–1692.

[12] A. Papoulis, Probability, Random Variables and Stochastic Process, McGraw-Hill, New York, 1965.